4. LIMIT CYCLE PIO ANALYSIS with ASYMMETRIC SATURATION

An analysis of the PIO characteristics of aircraft can be made using the methods described in Chapter 3. As stated previously, PIO events are believed to be limit cycles created by the dynamic interaction of the pilot-aircraft system. This fact requires that a model of both the pilot and aircraft be created in order to simulate PIO behavior.

The DIDF prediction method offers an excellent means of examining the individual effect of each nonlinearity present in the pilot-aircraft system. The diagonal elements of the N_A matrix allows the activity of each nonlinearity to be clearly seen. Furthermore, the DIDF prediction method helps ensure that no limit cycle solutions are overlooked. The discovery of limit cycles using simulation depends on guessing proper initial conditions. These initial conditions can be properly determined by the oscillatory state variable, x_s, given by the DIDF prediction method. Once proper initial conditions are determined, it is possible to use simulation to validate limit cycles predicted by the DIDF method.

Since we are mainly interested in the effects of simultaneous multiple asymmetric saturation, we will concentrate our efforts in this area. An aircraft that has a number of asymmetric nonlinearities will be chosen for study. Saturation elements will be studied for simultaneous and independent behavior.

Nonlinear effects that will be studied include asymmetric stick limiting, asymmetric elevator deflection limiting, and elevator rate limiting. These effects will be studied for independent and simultaneous behavior in order to gain insight into the independent and coupled characteristics of each.

4.1 PIO Analysis with Asymmetric Stick Limits

Control stick movement is almost always limited asymmetrically in the longitudinal axis because the stick is permitted to move farther aft than forward. Therefore, it is desirable to investigate the effects of asymmetric stick limiting on PIO characteristics. The NT-33A is variable stability aircraft used by the United States Air Force to investigate the effects of various configurations of aircraft and flight control systems on aircraft flight dynamics. A pilot-aircraft model based on the NT-33A can be described by the following block diagram:[28]

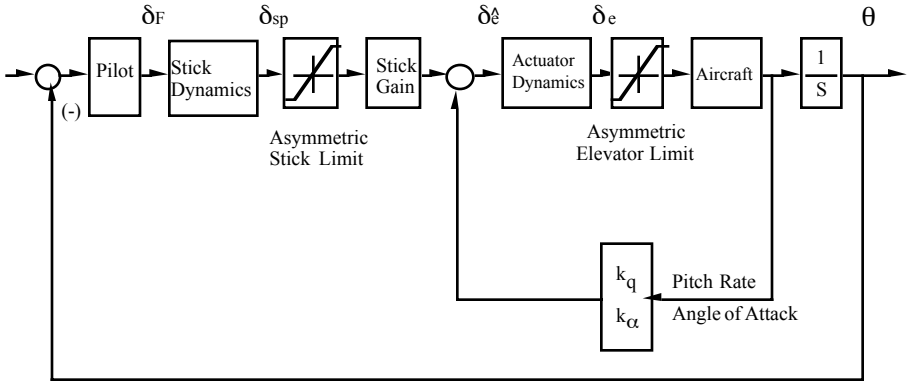

Figure 4.1.1 Block Diagram of NT-33A with Active Control System and Asymmetric Stick Limits

It can be seen from Figure 4.1.1 that a pitch rate and angle-of-attack control system is employed. The bare airframe dynamics are given by

$$\begin{Bmatrix}\dot{\alpha}\\ \dot{q}\end{Bmatrix} = \begin{bmatrix}-1.31 & 1.00\\ -3.21 & -1.65\end{bmatrix}\begin{Bmatrix}\alpha\\ q\end{Bmatrix} + \begin{bmatrix}-0.05\\ -10.29\end{bmatrix}\delta_e \qquad (4.1.1)$$

where pitch rate (q) is in units of deg/s, angle-of-attack (α) is in deg, and elevator deflection (δ_e) is in units of deg. This aircraft has a damping ratio of, $\zeta = 0.6$ and a natural

frequency of, $\omega_n = 2$ rad/s. These airframe dynamics are augmented by two feedback paths where, $k_q = 0.32$ and $k_\alpha = 1.0$. This feedback increases both damping ratio and natural frequency of the bare airframe.

Actuator dynamics are given by,

$$\frac{\delta_e}{\delta_{\hat{e}}} = \frac{75^2}{s^2 + 2(0.7)(75)s + 75^2} \qquad \text{(deg/deg)} \qquad (4.1.2)$$

and stick dynamics are given by,

$$\frac{\delta_{sp}}{\delta_F} = \frac{23^2 / 22}{s^2 + 2(0.65)(23)s + 23^2} \qquad \text{(in/lb)} \qquad (4.1.3)$$

and the stick gain is -16.51 deg / in.

It will be assumed that the pilot controls pitch attitude, θ. The pilot will be modeled as a gain,

$$\frac{\delta_F}{\theta} = k_p \qquad \text{(lb/deg)} \qquad (4.1.4)$$

This synchronous pilot model should be a sufficient representation of the pilot since we are mainly concerned with the effects of asymmetric limiting, and not attempting to replicate a particular PIO event.

The limits of stick position are $d_U = +3.6$ inches and $d_L = -2.0$ inches. Positive position is aft stick displacement. These limits will be represented by DIDF with parameters, d and c, defined from equations 3.2.1 and 3.2.2 as

$$d = 2.8 \text{ in} \qquad (4.1.5)$$

$$c = 0.8 \text{ in} \tag{4.1.6}$$

A state space model of this pilot-aircraft system can be created in which the state variables are,

$$x = \begin{Bmatrix} \alpha & \text{(deg)} \\ q & \text{(deg/s)} \\ \theta & \text{(deg)} \\ \delta_{sp} & \text{(in)} \\ \dot{\delta}_{sp} & \text{(in/s)} \\ \delta_e & \text{(deg)} \\ \dot{\delta}_e & \text{(deg/s)} \end{Bmatrix} \tag{4.1.7}$$

The corresponding F, G, and H matrices are shown in Table 4.1.1,

Table 4.1.1 State Space Model for NT-33A Asymmetric Stick Limit PIO Analysis

F=

-1.31	1.00	-0.05	0.00	0.00	0.00	0.00
-3.21	-1.65	-10.29	0.00	0.00	0.00	0.00
0.00	1.00	0.00	0.00	0.00	0.00	0.00
0.00	0.00	0.00	0.00	0.00	0.00	1.00
0.00	0.00	0.00	0.00	-kp(24.05)	-529.00	-29.90
0.00	0.00	0.00	1.00	0.00	0.00	0.00
5625.00	1800.00	-5625.00	-105.00	0.00	0.00	0.00

G=

0.00
0.00
0.00
0.00
0.00
0.00
-92865.38

H=

0.00	0.00	0.00	1.00	0.00	0.00	0.00

It can be seen from Figure 4.1.1 that, $\hat{y} = \delta_{sp}$ and $\hat{u}$ is the input to the stick gain element.

A linear analysis of this system (without saturation) shows that instability occurs at a pilot gain of about 8.8 lb/deg. The unstable motion that occurs as a result of pilot gains above 8.8 lb/deg is limited by the stick limit. This limiting of unstable motion forms a limit cycle, and, therefore, a PIO is possible for pilot gains above about 8.8 lb/deg.

The characteristics of the PIO can be determined through the use of the prediction methods presented in Chapter 3. Simulated results can be obtained through the use of the

5th order Runge-Kutta numerical integration method. Limit cycle solutions were simulated by using initial conditions of 1 degree in pitch attitude.

Table 4.1.2 Simulated and Predicted Limit Cycle Solutions for The NT-33A with Asymmetric Stick Limiting

	SIMULATED					PREDICTED						
k_p	ω	$\lvert\theta_s\rvert$	$\lvert\delta e_s\rvert$	θ_c	δe_c	ω	$\lvert\theta_s\rvert$	$\lvert\delta e_s\rvert$	θ_c	δe_c	N_A	N_B
9	8.44	5.34	37.0	0.12	0.11	8.49	5.33	36.5	0.05	0.0	0.98	0.97
10	8.44	6.26	44.5	0.45	0.16	8.49	6.10	41.7	0.39	0.0	0.83	0.82
11	8.44	6.89	49.7	0.94	0.14	8.49	6.52	44.6	0.73	0.0	0.80	0.69
12	8.28	7.42	54.1	1.41	0.15	8.49	6.82	46.7	1.05	0.0	0.74	0.58
14	8.13	8.03	60.0	2.00	0.18	8.49	7.25	49.6	1.63	0.0	0.63	0.44
16	8.13	8.30	63.0	2.25	0.16	8.49	7.46	51.1	1.97	0.0	0.55	0.36
18	8.13	8.46	64.9	2.41	0.17	8.49	7.57	51.8	2.20	0.0	0.49	0.31
20	8.13	8.57	66.5	2.53	0.29	8.49	7.64	52.3	2.36	0.0	0.44	0.27

The results of simulated and predicted methods of solution for the NT-33A model with asymmetric stick limiting are shown in Table 4.1.2. Table 4.1.2 shows simulated results on the left hand side and the corresponding predicted results on the right. Pilot gain is shown on the far left column and ranges from 9 to 20 lb/deg. Oscillation frequency, in rad/s, is shown in the first column of data, followed by amplitude of pitch attitude and amplitude of elevator deflection in degrees. Mean points of oscillation for

pitch attitude and elevator deflection are shown in degrees in the next two columns. The far right columns show the amount of saturation, N_A, and the amount of offset limiting, N_B, present in each oscillation.

Inspection of the values of N_A and N_B show that for small values of pilot gain , k_p, the stick deflection is limited only slightly. This result is expected and as pilot gain increases the amount of limiting should and does increase.

Although other variables can be computed, the oscillation of the aircraft will be discussed in terms of pitch attitude. Frequencies of oscillation and the nature of the pitch attitude oscillations are shown in Figures 4.1.2 through 4.1.4.

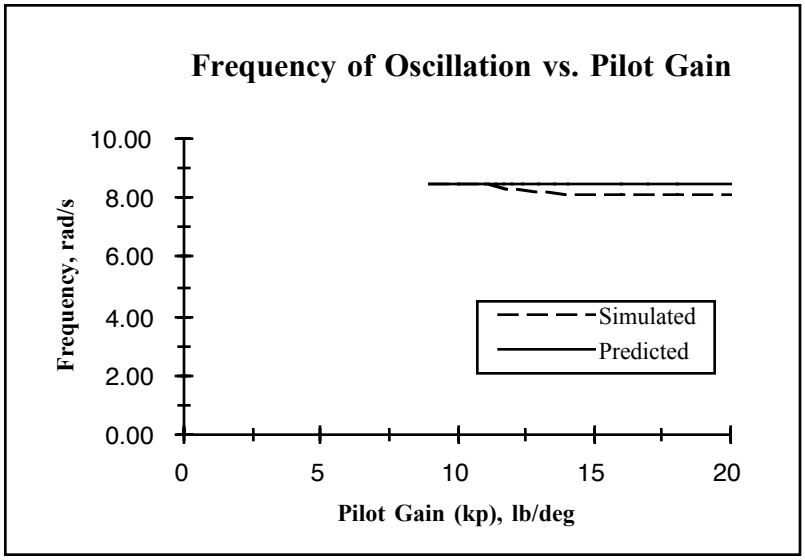

Figure 4.1.2 Frequency of Oscillation for NT-33A with Asymmetric Stick Limit

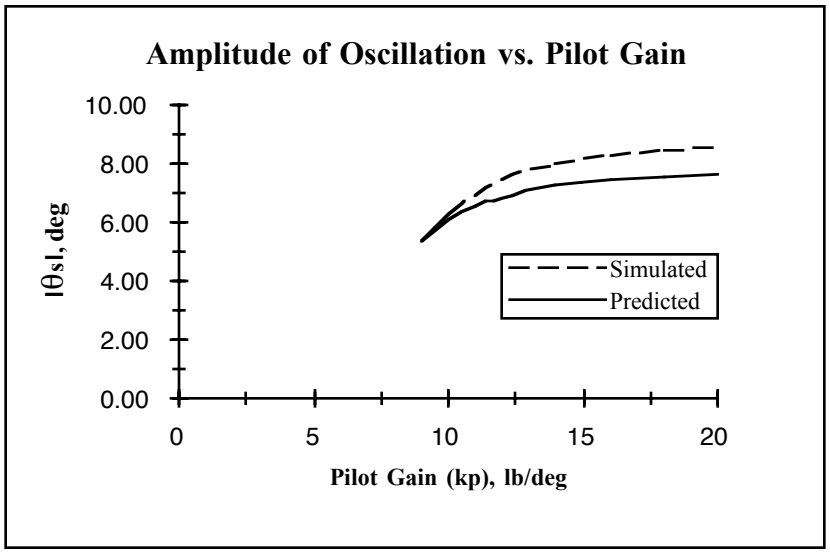

Figure 4.1.3 Pitch Attitude Amplitude of Oscillation for NT-33A with Asymmetric Stick Limit

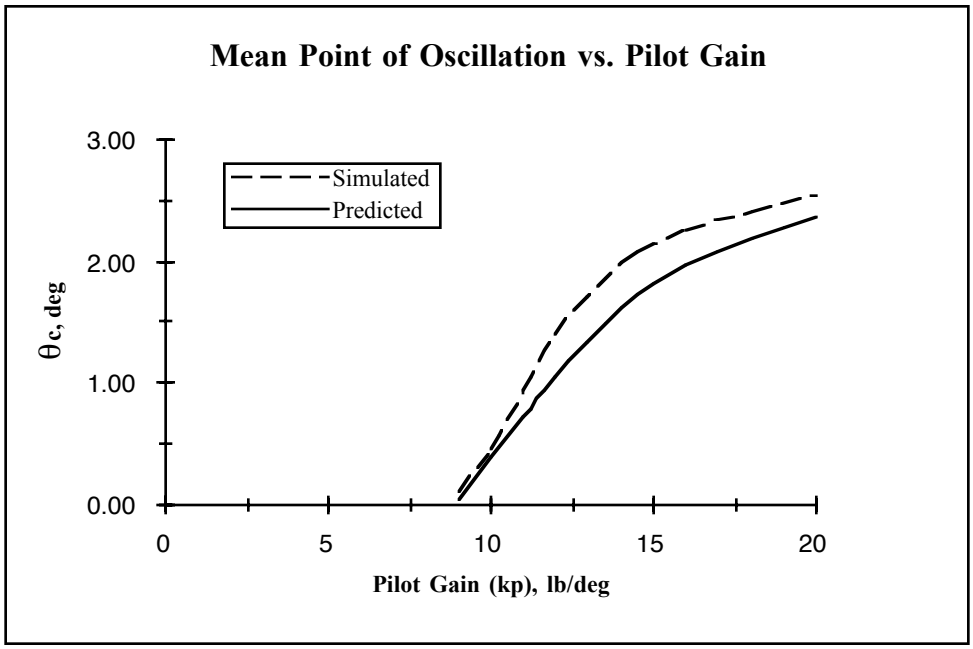

Figure 4.1.4 Pitch Attitude Mean Point of Oscillation for NT-33A with Asymmetric Stick Limit

Upon examination of the nature of the limit cycle oscillations, it can be seen that the frequencies of oscillation seem to vary only slightly for varied pilot gain. However,

changes in pilot gain cause both oscillation amplitude and oscillation offset to change significantly. The region of low pilot gain (below 11 lb/deg) is characterized by large changes in amplitude and offset for relatively low changes in pilot gain. In other words, if the pilot's behavior changes only slightly the effects can be seen dramatically in the nature of the oscillation. As pilot gain is increased further the offset increases dramatically with respect to the magnitude of oscillation. In the particular case of $k_p = 20$ lb/deg, the offset is more than 24% of the amplitude of oscillation. These facts reveal that any changes in pilot behavior as a function of time can cause dramatic changes in oscillation characteristics.

We are also interested in the elevator oscillations which occur as a result of the pilot input. Large amplitudes of oscillation of elevator deflection may reach values such that limiting will occur. This situation may cause the characteristics of the overall aircraft oscillation to change. The behavior of the elevator during an oscillation due to stick limiting is presented in Figures 4.1.5 and 4.1.6.

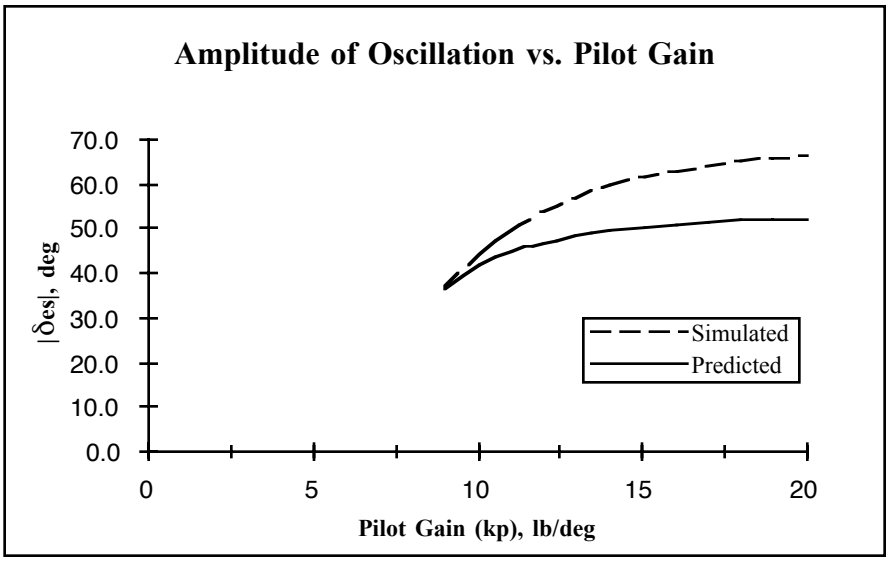

Figure 4.1.5 Elevator Amplitude of Oscillation for NT-33A with Asymmetric Stick Limit

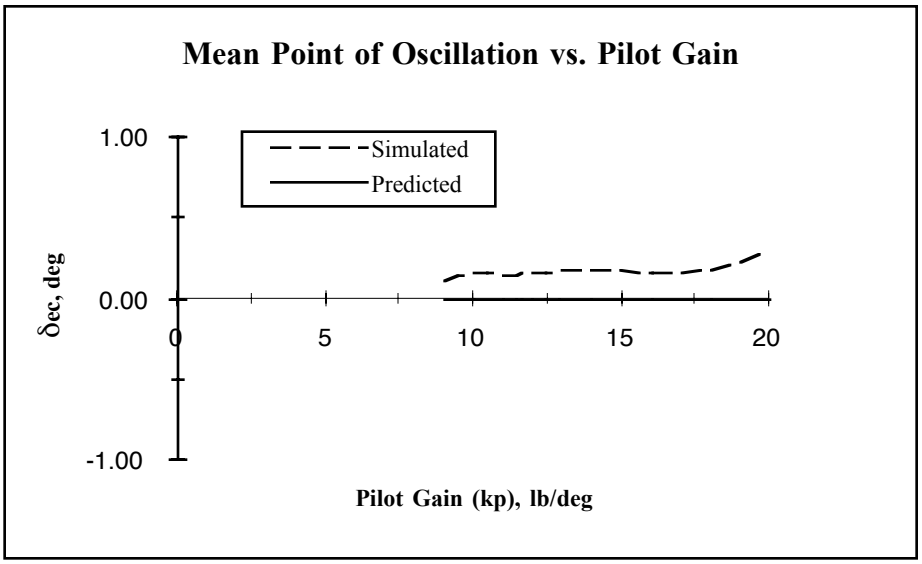

Figure 4.1.6 Elevator Mean Point of Oscillation for NT-33A with Asymmetric Stick Limit

It can be seen from Figure 4.1.5 that stick limiting produces excessive elevator travel. Elevator travel is usually limited in amplitude to about 20 degrees of deflection,

however these oscillations produce elevator deflection amplitudes of almost 40 degrees even for lower values of pilot gain. Clearly, these values would be significantly limited by the elevator travel limits. This result suggests a need for the introduction of both elevator and stick limits into the model of the pilot-aircraft system.

Figure 4.1.6 demonstrates the DIDF method's inability to predict mean point of oscillation for elevator deflection. As stated in Section 3.6, the use of the DIDF prediction method causes predictions of zero mean points of oscillation for state variables that are the derivative of another state variable. In this case, δ_e is not the derivative of a state variable, but it is coupled with the state variables $\dot{\delta}_e$ and $\dot{\delta}_{sp}$, which can be seen from examination of the fifth row of the F matrix. This coupling of δ_e with derivative state variables causes the prediction of δ_{ec} to be zero for all values of k_p.

Although not all components of the oscillation are accurately predicted, the overall result of the prediction method produces acceptable results. Frequency, amplitude, and mean point of oscillation of the aircraft during these oscillations match quite well with simulated results.

4.2 PIO Analysis with Asymmetric Stick and Asymmetric Elevator Deflection Limits

The model of Figure 4.2.1 needs only to be modified slightly to introduce an elevator deflection limit in addition to the existing stick position limit. A saturation element is placed after the actuator dynamics to represent the asymmetric elevator deflection limit. This modification can be seen in Figure 4.2.1.

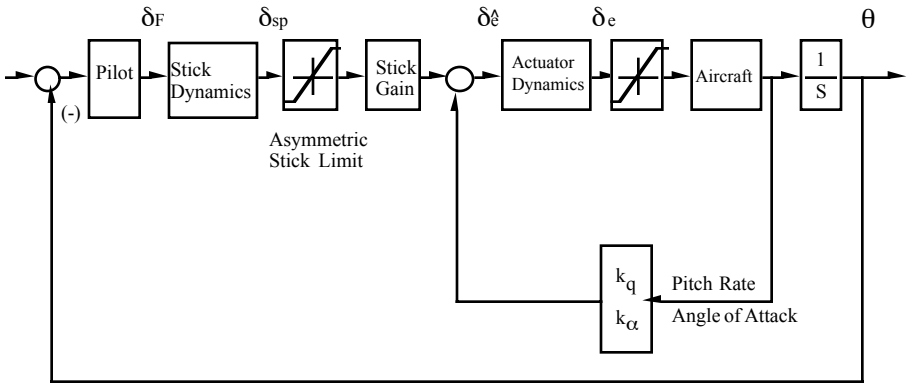

Figure 4.2.1 Block Diagram of NT-33A with Active Control System and Asymmetric Stick and Elevator Deflection Limits

where all transfer function blocks in Figure 4.2.1 are defined as they were previously in Section 4.1.

The definition of the state space model begins with the construction of the input and output vector to the nonlinear elements. There are two nonlinear elements in this case. Therefore, the input vector, $\hat{y}$, has a dimension of 2 x 1, and the output vector, has a dimension of 2 x 1. Additionally, the N_A and N_B matrices are diagonal by definition, and in this case, will have a dimension of 2 x 2. This system of equations can be defined by

$$\begin{Bmatrix} u_1 \\ u_2 \end{Bmatrix} = \begin{bmatrix} N_1 & 0 \\ 0 & N_2 \end{bmatrix} \begin{Bmatrix} y_1 \\ y_2 \end{Bmatrix} \tag{4.2.1}$$

where

$$\begin{Bmatrix} \hat{u}_1 \\ \hat{u}_2 \end{Bmatrix} = \begin{Bmatrix} u_1 \\ u_2 \end{Bmatrix} + \begin{Bmatrix} c_1 \\ c_2 \end{Bmatrix} \tag{4.2.2}$$

and

$$\begin{Bmatrix} \hat{y}_1 \\ \hat{y}_2 \end{Bmatrix} = \begin{Bmatrix} y_1 \\ y_2 \end{Bmatrix} + \begin{Bmatrix} c_1 \\ c_2 \end{Bmatrix} \quad (4.2.3)$$

The input to the asymmetric stick limit is $\hat{y}_1$, and the output is $\hat{u}_1$. Therefore, the value of N_{A1} indicates the amount of stick limiting present in a given oscillation. The input to the asymmetric elevator limit is $\hat{y}_2$, and the output is $\hat{u}_2$. The value of N_{A2} indicates the amount of elevator limiting present in a given oscillation.

The stick limits are the same as those given in Section 4.1 and are given by the parameters d_1 and c_1. The limits of elevator deflection are d_{U2} = 15.0 deg and d_{L2} = -25.0 deg. The elevator deflection limits are given by the parameters d_2 and c_2. Through the use of equations 3.2.1 and 3.2.2 the limits may be described by

d_1= 2.8 inches (4.2.4)

c_1 = 0.8 inches (4.2.5)

and

d_2 = 20 degrees (4.2.6)

c_2 = -5.0 degrees (4.2.7)

A state space model can now be arranged such that the states correspond to equation 4.1.5. The F, G, and H matrices are shown in Table 4.2.1.

Table 4.2.1 State Space Model for NT-33A Asymmetric Stick Position and Asymmetric Elevator Deflection Limit PIO Analysis

F=

-1.31	1.00	0.00	0.00	0.00	0.00	0.00
-3.21	-1.65	0.00	0.00	0.00	0.00	0.00
0.00	1.00	0.00	0.00	0.00	0.00	0.00
0.00	0.00	0.00	0.00	1.00	0.00	0.00
0.00	0.00	-kp(24.05)	-529.00	-29.90	0.00	0.00
0.00	0.00	0.00	0.00	0.00	0.00	1.00
5625.00	1800.00	0.00	0.00	0.00	-5625.00	-105.00

G=

0.00
0.00
0.00
0.00
0.00
0.00
-92865.38

-0.05
-10.29
0.00
0.00
0.00
0.00
0.00

H=

0.00	0.00	0.00	1.00	0.00	0.00	0.00
0.00	0.00	0.00	0.00	0.00	1.00	0.00

As in the stick limit system, the linearized stick and elevator limit system becomes unstable at a pilot gain of about 8.8 lb/deg. The stick and elevator deflection limiting cause limit cycle behavior to occur for pilot gains above 8.8 lb/deg. Therefore, PIO is possible for pilot gains above 8.8 lb/deg.

Once again, the nature of the PIO may be determined through the use of the DIDF method of Chapter 3. Simulated results were obtained by use of the 5th order Runge-Kutta integration scheme using the initial conditions defined in Section 4.1. Results of the

simulated method with a time step of 0.01 sec and the DIDF prediction method are shown in Tables 4.2.2 and 4.2.3.

Table 4.2.2 Simulated and Predicted Limit Cycle Solutions for the NT-33A with Asymmetric Stick Position and Asymmetric Elevator Deflection Limiting

	SIMULATED				PREDICTED					
k_p	ω	$\lvert\theta_s\rvert$	$\lvert\delta e_s\rvert$	$\lvert\delta sps\rvert$	ω	$\lvert\theta_s\rvert$	$\lvert\delta e_s\rvert$	$\lvert\delta sps\rvert$	N_{A1}	N_{A2}
9	8.28	2.60	18.3	1.08	8.35	2.60	18.2	1.77	1.00	0.95
10	7.67	3.91	30.8	1.80	7.75	3.67	28.7	1.69	1.00	0.73
11	7.21	4.62	37.0	2.34	7.58	3.96	32.1	2.00	0.94	0.67
12	6.90	5.16	41.6	2.86	7.51	4.08	33.6	2.25	0.88	0.65
14	6.44	6.01	49.7	3.87	7.41	4.22	35.5	2.71	0.77	0.62
16	6.14	6.65	56.5	4.90	7.34	4.34	37.3	3.19	0.69	0.59
18	5.83	7.14	59.4	5.91	7.33	4.36	37.6	3.61	0.61	0.59
20	5.68	7.54	61.3	6.94	7.30	4.41	38.3	4.05	0.56	0.58

Table 4.2.3 Simulated and Predicted Limit Cycle Solutions for the NT-33A with Asymmetric Stick Position and Asymmetric Elevator Deflection Limiting

	SIMULATED			PREDICTED				
k_p	θ_c	δ_{ec}	δ_{spc}	θ_c	δ_{ec}	δ_{spc}	N_{B1}	N_{B2}
9	0.10	0.69	-0.02	0.08	0.51	-0.03	1.00	0.91
10	0.71	5.22	-0.30	0.59	4.44	-0.27	1.00	0.53
11	1.04	6.37	-0.50	0.86	6.09	-0.43	0.95	0.45
12	1.33	6.45	-0.66	1.02	6.77	-0.56	0.89	0.42
14	1.66	4.54	-1.03	1.28	7.59	-0.81	0.78	0.40
16	1.98	2.87	-1.34	1.53	8.33	-1.11	0.68	0.38
18	2.22	1.75	-1.71	1.66	8.47	-1.36	0.61	0.37
20	2.32	1.34	-2.04	1.81	8.75	-1.65	0.54	0.36

Table 4.2.2 shows simulated and predicted results for amplitudes of the limit cycle oscillation. Pilot gain, k_p, is shown in the first column and ranges from 9 to 20 lb/deg. Amplitude of pitch attitude oscillation in degrees is shown in the first column of data, followed by, amplitude of elevator deflection (before limiting) in degrees and amplitude of stick position (before limiting) in inches. The last columns show the amounts of saturation in each of the two saturation element. Recall N_{A1} corresponds to the amount of stick limiting and N_{A2} corresponds to the amount of elevator deflection limiting.

Table 4.2.3 shows simulated and predicted mean points of oscillation during the limit cycle. Once again, pilot gain is shown in the first column. The first data column is the mean point of oscillation of pitch attitude in degrees, followed by mean points of oscillation of elevator deflection (before limiting) in degrees and stick position (before limiting) in inches. The last two columns refer to the amount of offset occurring in the each saturation element. N_{B1} corresponds to the stick position limit and N_{B2} corresponds to the elevator deflection limit.

Notice in Tables 4.2.2 and 4.2.3 that the N_{A1} and N_{B1} elements are unity for pilot gains up to and including 10 lb/deg. This means that limiting is only occurring in the elevator deflection saturation element. The pilots commands to the stick are not limited at all during these potential limit cycles. As pilot gain is increased beyond about 10 lb/deg, both saturation elements become active, and both stick position and elevator deflection become limited.

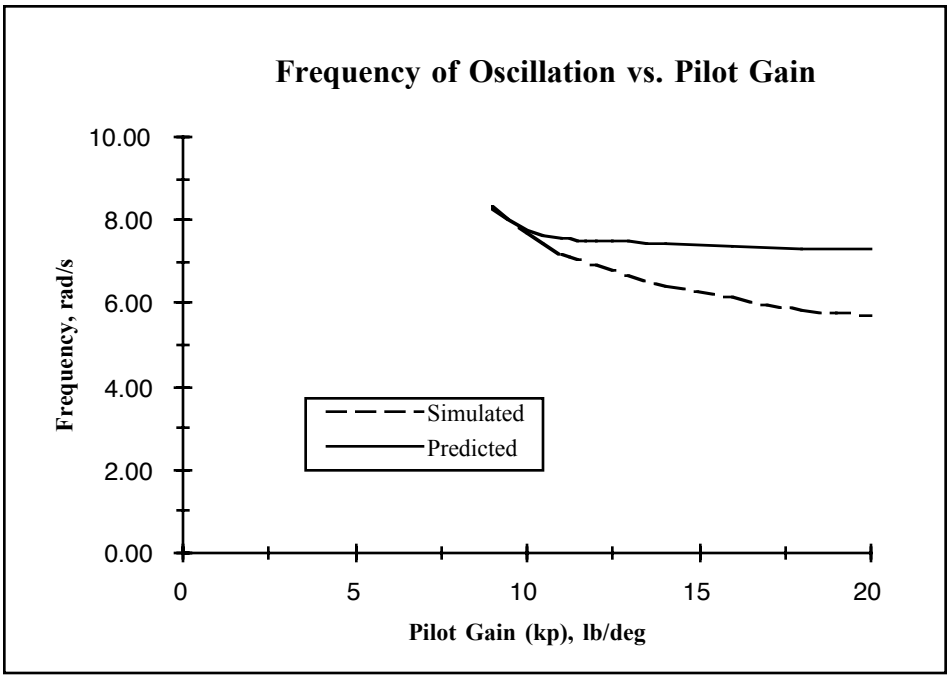

Figure 4.2.1 Frequency of Oscillation for NT-33A with Asymmetric Stick Position and Asymmetric Elevator Deflection

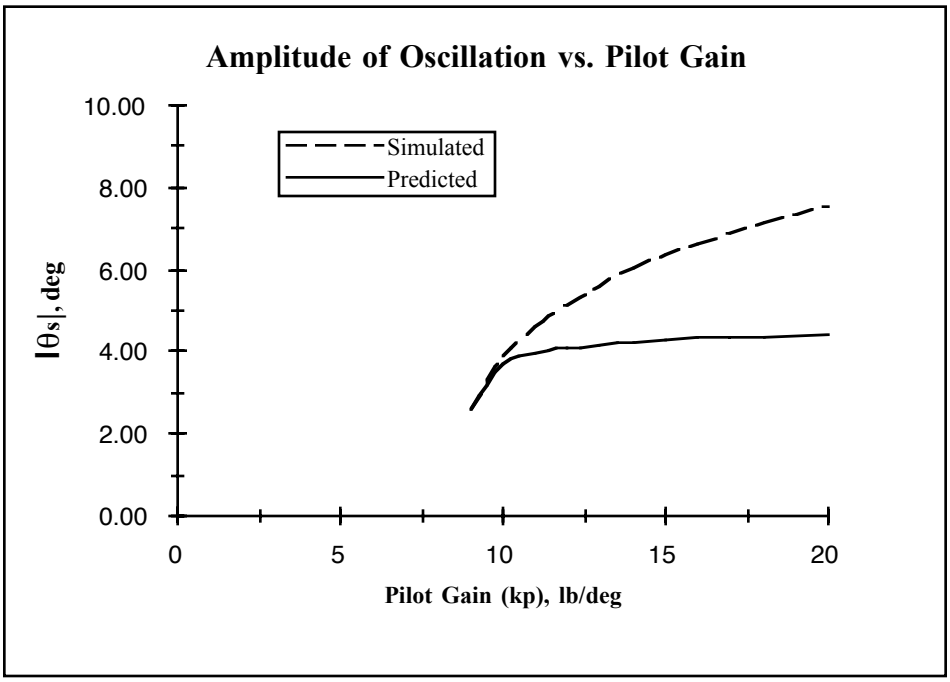

Figure 4.2.2 Amplitude of Pitch Attitude Oscillation for NT-33A with Asymmetric Stick Position and Asymmetric Elevator Deflection

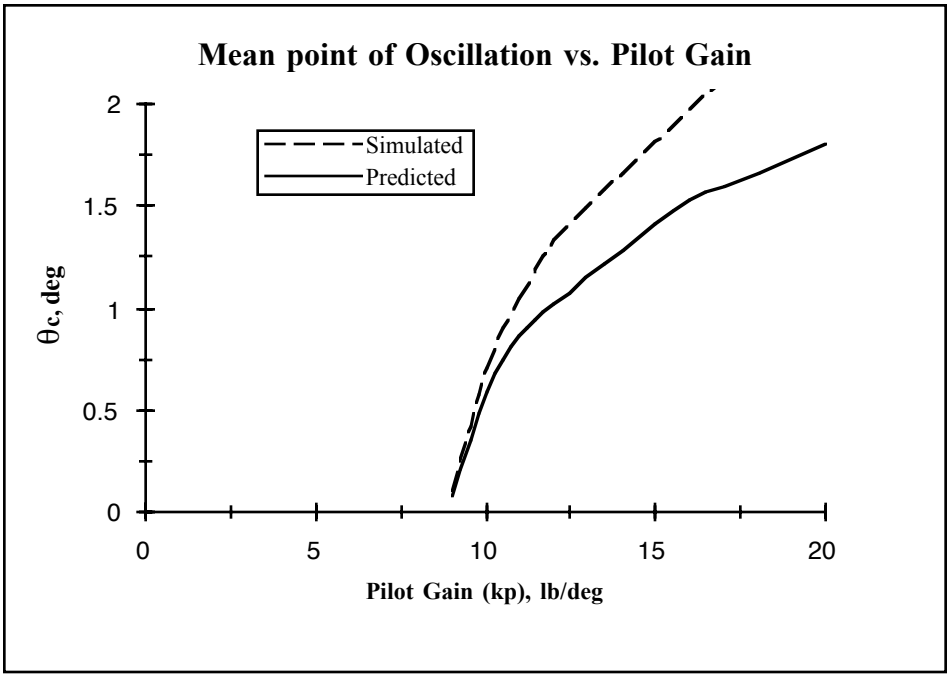

Figure 4.2.3 Mean point of Pitch Attitude Oscillation for NT-33A with Asymmetric Stick Position and Asymmetric Elevator Deflection

The frequency, amplitude and mean point of oscillation of the aircraft during these PIO events are shown in Figures 4.2.1 through 4.2.3. Figure 4.2.1 shows a comparison of simulated and predicted frequencies of oscillation over a range of pilot gains. Predicted and simulated values match fairly well, and are quite close for the cases of small amounts of saturation. This oscillation is predicted to have a frequency between 7 and 8 rad/s for a wide range of pilot gains.

Figures 4.2.2 and 4.2.3 show simulated and predicted amplitude and mean point of oscillation of aircraft pitch attitude over a range of pilot gains. Both amplitude and mean point of oscillation increase rapidly for small values of pilot gain (k_p = 9 - 10 lb/deg). As pilot gain is increased further, the affects of changing pilot gain are not as dramatic;

however, the nature of the PIO continues to change. Amplitude of oscillation seems to level off, but the mean point of oscillation continues to rise with increasing pilot gain.

It can be seen that the characteristics of this PIO will change as pilot gain changes. The frequency will vary only slightly, however the motion of the aircraft can change tremendously with changing pilot gain. An examination of the commanded stick position and elevator deflection can be made in an effort to gain a further understanding of the mechanics of this PIO.

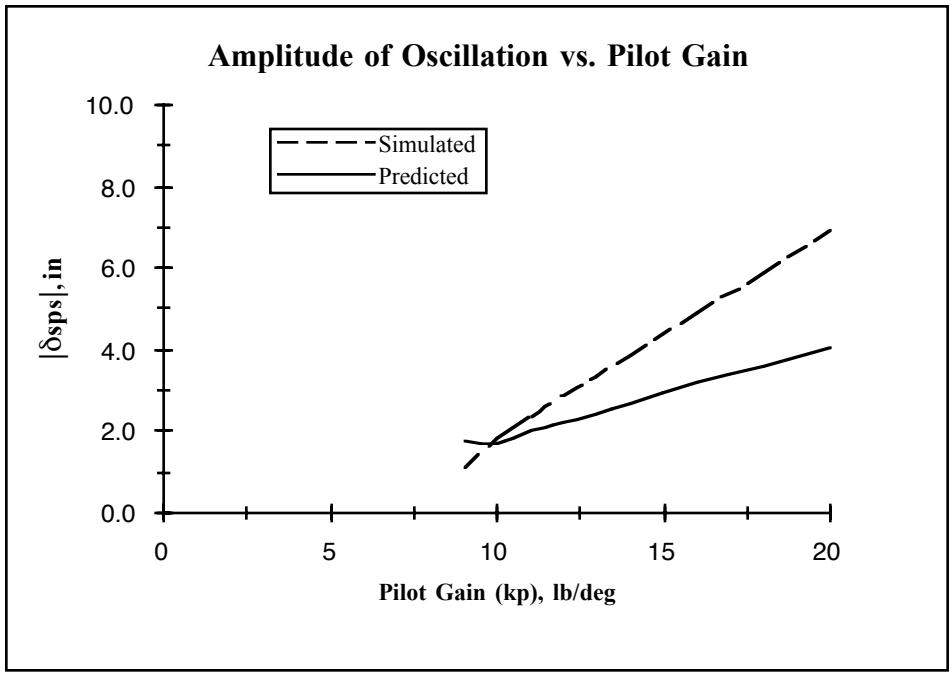

Figure 4.2.4 Amplitude of Stick Position Oscillation for NT-33A with Asymmetric Stick Position and Asymmetric Elevator Deflection

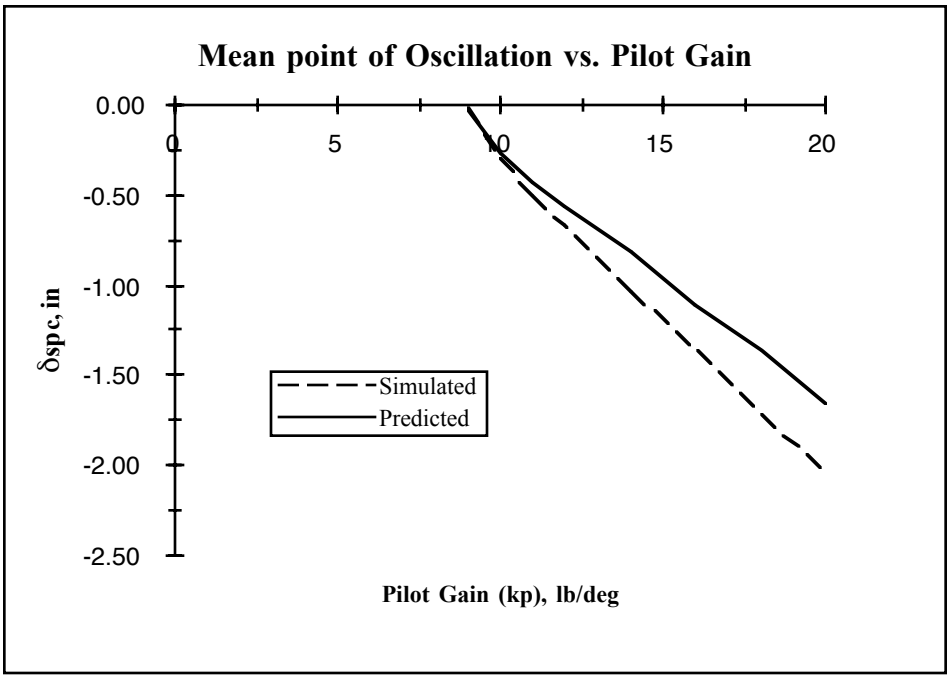

Figure 4.2.5 Mean point of Stick Position Oscillation for NT-33A with Asymmetric Stick Position and Asymmetric Elevator Deflection

Figure 4.2.4 shows the simulated and predicted amplitude of stick position oscillation for a range of pilot gains. It can be seen that amplitude increases steadily as pilot gain is increased. Figure 4.2.5 shows simulated and predicted mean point of stick position oscillation for a range of pilot gains. It can be seen that the mean point of oscillation becomes increasingly negative as pilot gain is increased. This result suggests that the pilot is increasing the pitch attitude as pilot gain increases, which is consistent with Figure 4.2.3.

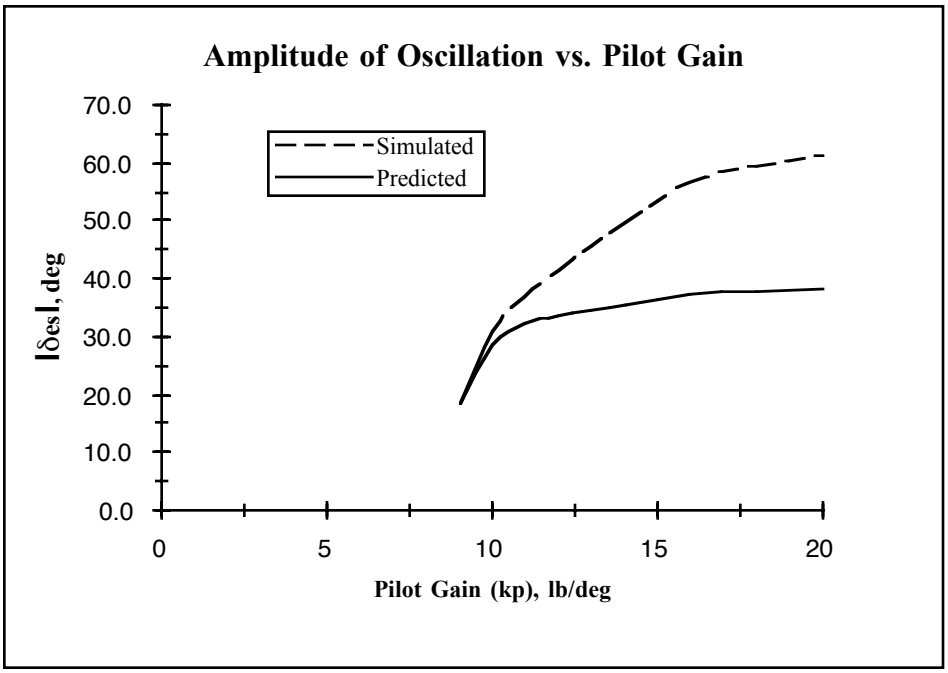

Figure 4.2.6 Amplitude of Elevator Deflection Oscillation for NT-33A with Asymmetric Stick Position and Asymmetric Elevator Deflection

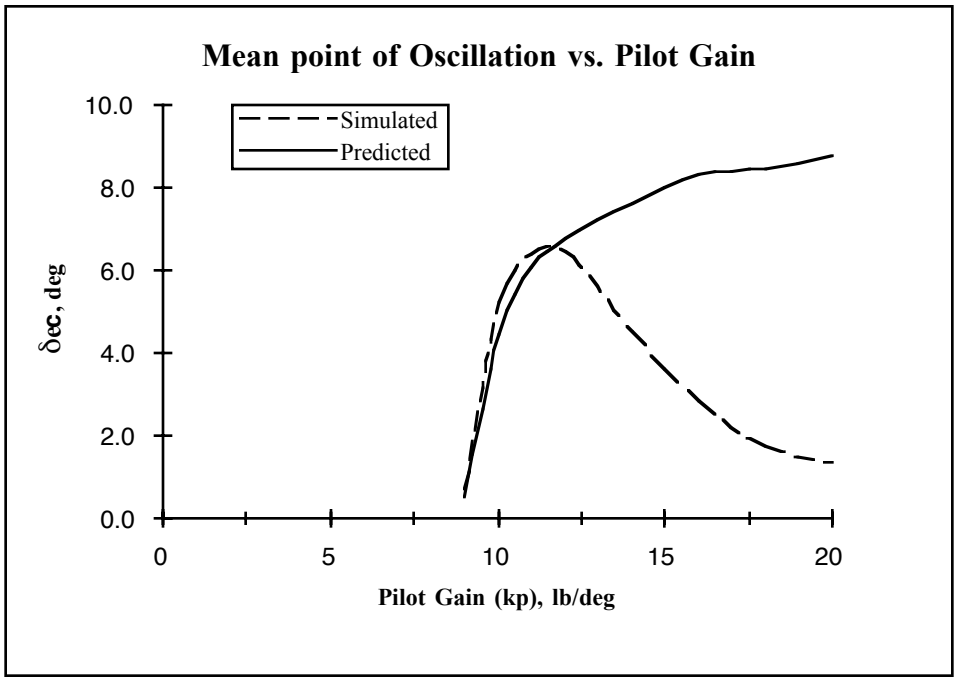

Figure 4.2.7 Mean point of Elevator Deflection Oscillation for NT-33A with Asymmetric Stick Position and Asymmetric Elevator Deflection

Figure 4.2.6 shows the simulated and predicted amplitude of elevator deflection oscillation for a range of pilot gains. It can be seen that amplitude increases dramatically in the region of low pilot gain (8 -10 lb/deg) and begins to taper off as pilot gain is increased.

Figure 4.2.7 shows the simulated and predicted mean point of elevator deflection oscillation for a range of pilot gains. Once again, the region of low pilot gain (8 - 10 lb/deg) is characterized by dramatic changes in the mean point of oscillation. As pilot gain is increased the predicted mean point of oscillation begins to level off, but the simulated mean point of oscillation migrates back towards zero. This phenomenon can be investigated by examination of the elevator oscillations. Phase portraits of the elevator oscillations for increasing values of pilot gain can be seen in Figures 4.2.8 and 4.2.9.

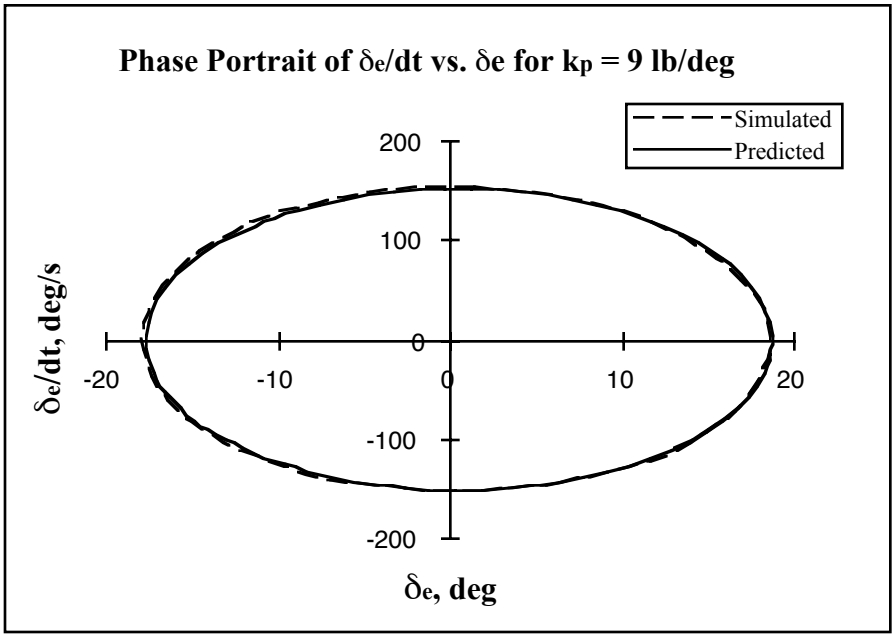

Figure 4.2.8 Phase Portrait of Elevator Oscillation for Pilot Gain, k_p = 9 lb/deg

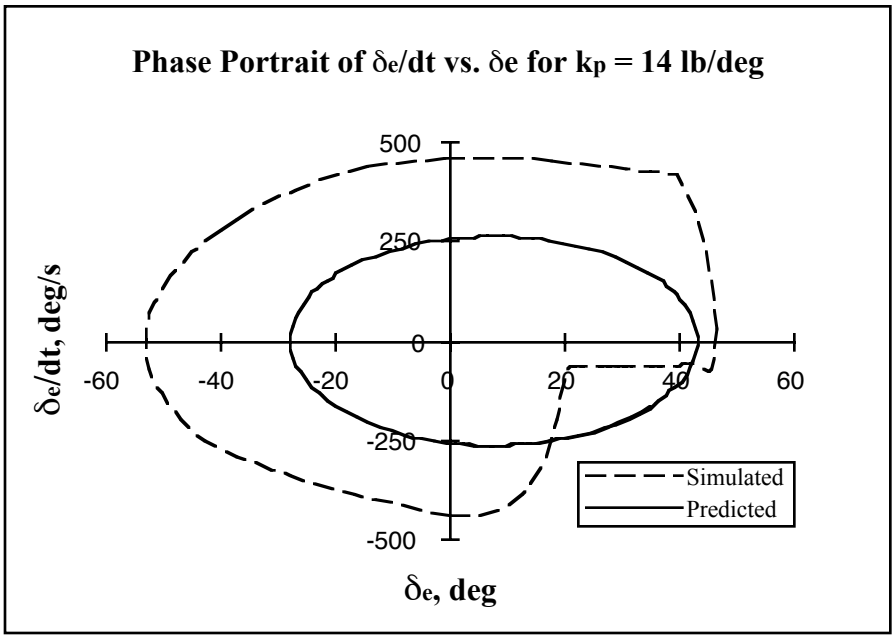

Figure 4.2.9 Phase Portrait of Elevator Oscillation for Pilot Gain, k_p = 14 lb/deg

Figure 4.2.8 shows the oscillation of the elevator for a pilot gain of 9 lb/deg. This case shows that the simulated limit cycle has an elliptic shape and is predicted quite accurately by the DIDF method. Figure 4.2.9 shows that, for a pilot gain of 14 lb/deg, the actual elevator limit cycle oscillation is not elliptical and is not accurately represented by the ellipse approximation given by the DIDF method. This discrepancy in simulated and predicted elevator limit cycle oscillation shape explains the behavior shown in Figure 4.2.5. As pilot gain increases, the limit cycle oscillations become highly nonlinear, and the DIDF method becomes less accurate. This situation causes the predicted amplitude and mean points of oscillation to vary from the simulated values.

It can also be seen in Figures 4.2.8 and 4.2.9 that the elevator rate is quite high even for low pilot gains. The NT-33A has a physical elevator rate limit of about 157

deg/s, which would likely be exceeded during these limit cycles. Therefore, it is desirable to incorporate an elevator rate limit into the NT-33A pilot-vehicle model. This combination will allow a detailed examination of the dynamics involved in the behavior of the NT-33A during PIO.

4.3 PIO Analysis with Asymmetric Stick Position Limits, Asymmetric Elevator Deflection Limits and Elevator Rate limits

An elevator rate limit is added to the system of Section 4.2 by adding a limiter within the actuator dynamics. This addition is made by rearranging the block diagram of Figure 4.2.1 as shown ini Figure 4.3.1. The rate and deflection limited actuator dynamics are given by the block diagram of Figure 4.3.2.

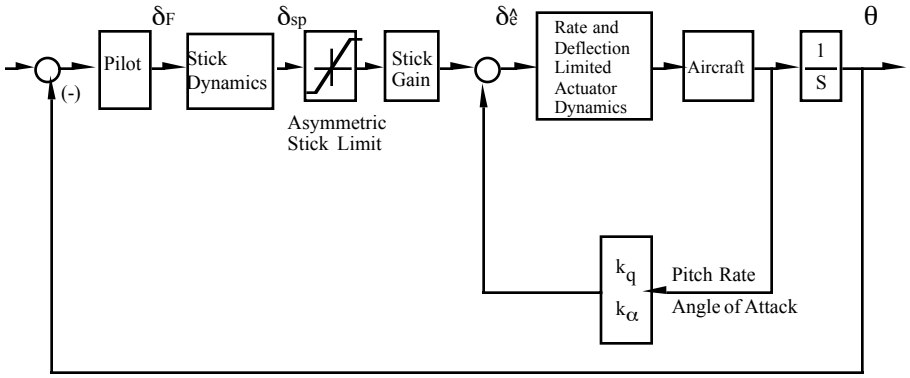

Figure 4.3.1 Block Diagram of NT-33A with Active Control System and Asymmetric Stick Position Limits, Asymmetric Elevator Deflection Limits, and Elevator Rate limits

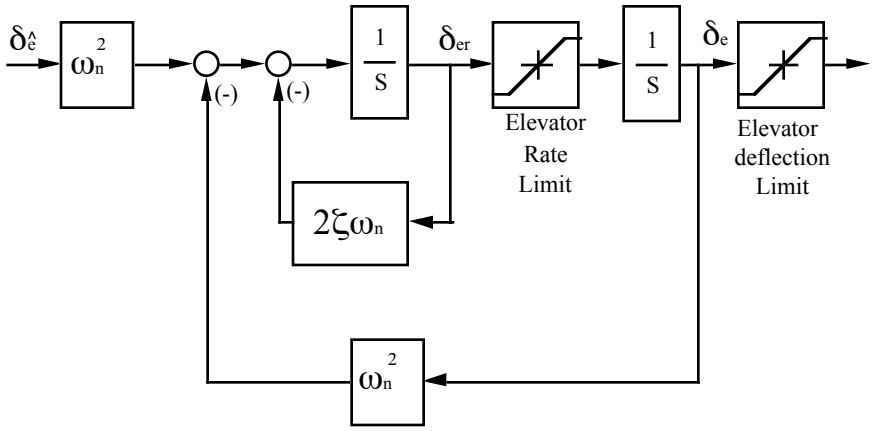

Figure 4.3.2 Block Diagram of Actuator Dynamics with Rate and Asymmetric Deflection Limiting

The block diagram of Figure 4.3.1 shows the actuator dynamics with rate and deflection limiters implemented within it. The block diagram of Figure 4.3.2 shows how these limits are implemented. The prelimited elevator rate is represented by δ_{er} and the prelimited elevator deflection is represented by δ_e. Otherwise, the dynamics of the elevator actuator will be the same as in Sections 4.1 and 4.2. Therefore, the natural frequency and damping ratio of the actuator are

$$\omega_n = 75 \text{ rad/s} \tag{4.3.1}$$

and

$$\zeta = 0.7 \tag{4.3.2}$$

Once again, a state space model can be constructed from the block diagram of the pilot-aircraft system. First, the input and output vectors to the DIDF elements must be defined. The asymmetric stick position limit and asymmetric elevator deflection limit will

be arranged as in section 4.2. The elevator rate limit will be defined to have input, y_3, and output, u_3. The values of d_1, d_2, c_1, and c_2 will be given, once again, by equations 4.2.4 through 4.2.7. The elevator rate limit will be defined by

$$d_3 = 157 \text{ deg/s} \tag{4.3.3}$$

$$c_3 = 0 \text{ deg/s} \tag{4.3.4}$$

This system of inputs and outputs is defined by

$$\begin{Bmatrix} u_1 \\ u_2 \\ u_3 \end{Bmatrix} = \begin{bmatrix} N_1 & 0 & 0 \\ 0 & N_2 & 0 \\ 0 & 0 & N_3 \end{bmatrix} \begin{Bmatrix} y_1 \\ y_2 \\ y_3 \end{Bmatrix} \tag{4.3.5}$$

where

$$\begin{Bmatrix} \hat{u}_1 \\ \hat{u}_2 \\ \hat{u}_3 \end{Bmatrix} = \begin{Bmatrix} u_1 \\ u_2 \\ u_3 \end{Bmatrix} + \begin{Bmatrix} c_1 \\ c_2 \\ c_3 \end{Bmatrix} \tag{4.3.6}$$

and

$$\begin{Bmatrix} \hat{y}_1 \\ \hat{y}_2 \\ \hat{y}_3 \end{Bmatrix} = \begin{Bmatrix} y_1 \\ y_2 \\ y_3 \end{Bmatrix} + \begin{Bmatrix} c_1 \\ c_2 \\ c_3 \end{Bmatrix} \tag{4.3.7}$$

A state space model may now be arranged which represents the block diagram structure of Figures 4.3.1 and 4.3.2. The state variables of this system will be given as

$$x = \begin{Bmatrix} \alpha & \text{(deg)} \\ q & \text{(deg/s)} \\ \theta & \text{(deg)} \\ \delta_{sp} & \text{(in)} \\ \dot{\delta}_{sp} & \text{(in/s)} \\ \delta_{er} & \text{(deg/s)} \\ \delta_e & \text{(deg)} \end{Bmatrix} \tag{4.3.5}$$

The corresponding F, G, and H matrices are shown in Table 4.3.1.

Table 4.3.1 State Space Model for NT-33A Asymmetric Stick Position, Asymmetric Elevator Deflection, and Elevator Rate Limit PIO Analysis

F=

-1.31	1.00	0.00	0.00	0.00	0.00	0.00
-3.21	-1.65	0.00	0.00	0.00	0.00	0.00
0.00	1.00	0.00	0.00	0.00	0.00	0.00
0.00	0.00	0.00	0.00	1.00	0.00	0.00
0.00	0.00	-kp(24.05)	-529.00	-29.90	0.00	0.00
5625.00	1800.00	0.00	0.00	0.00	-105.00	-5625.00
0.00	0.00	0.00	0.00	0.00	0.00	0.00

G=

0.00	-0.05	0.00
0.00	-10.29	0.00
0.00	0.00	0.00
0.00	0.00	0.00
0.00	0.00	0.00
-92865.38	0.00	0.00
0.00	0.00	1.00

H=

0.00	0.00	0.00	1.00	0.00	0.00	0.00
0.00	0.00	0.00	0.00	0.00	0.00	1.00
0.00	0.00	0.00	0.00	0.00	1.00	0.00

An analysis of the linearized system reveals that instability occurs at a pilot gain of about 8.8 lb/deg. Recall that this result is the same as the linearized models of Sections 4.1 and 4.2. Due to this fact, PIO can be expected for pilot gains greater than 8.8 lb/deg. These limit cycles will be a result of the stick position, elevator deflection, and elevator rate limiting of the unstable motion of the linear system. However, limit cycles also appear for pilot gains that are less thatn 8.8 lb/deg. This limit cycle behavior is induced

by the elevator rate limiting alone. A simulation of this behavior is possible by using the Runge-Kutta numerical integration scheme previously mentioned. Limit cycles can be initiated by using initial conditions of 10 degrees in angle-of-attack and pitch attitude. Tables 4.3.2 and 4.3.3 show simulated and predicted limit cycle solutions for this system.

Table 4.3.2 Simulated and Predicted Limit Cycle Solutions for the NT-33A with Asymmetric Stick Position, Asymmetric Elevator Deflection and Elevator Rate Limiting

	SIMULATED				PREDICTED						
k_p	ω	$\lvert\theta_s\rvert$	$\lvert\delta e_s\rvert$	$\lvert\delta sp_s\rvert$	ω	$\lvert\theta_s\rvert$	$\lvert\delta e_s\rvert$	$\lvert\delta sp_s\rvert$	N_{A1}	N_{A2}	N_{A3}
7	5.2	8.6	39.9	2.8	5.9	6.7	34.0	2.1	0.90	0.63	0.25
8	4.5	11.8	44.3	4.3	5.8	6.8	35.3	2.5	0.80	0.61	0.25
9	4.3	13.2	46.0	5.5	4.7	10.8	39.3	4.4	0.51	0.57	0.13
10	4.1	14.2	47.0	6.5	4.7	11.1	40.5	5.1	0.46	0.57	0.13
11	3.8	15.1	47.8	7.6	4.7	10.9	40.2	5.5	0.42	0.56	0.13
13	3.8	16.2	48.7	9.6	4.7	11.0	40.8	6.5	0.36	0.55	0.13
15	3.7	17.0	49.3	11.6	4.7	11.0	41.3	7.5	0.32	0.54	0.13

Table 4.3.2 shows frequency and amplitudes of limit cycle oscillations for a range of pilot gains. Pilot gains ranging from 7 to 15 lb/deg are shown in the first column. The first set of data in both the SIMULATED and PREDICTED portion of the table is frequency of oscillation in rad/s. The next three columns show amplitude of pitch attitude in degrees, elevator deflection in degrees, and stick position in inches. Predicted amounts of limiting in each of the saturation elements is shown in the last three columns.

Table 4.3.3 Simulated and Predicted Limit Cycle Solutions for the NT-33A with Asymmetric Stick Position, Asymmetric Elevator Deflection and Elevator Rate Limiting

	SIMULATED			PREDICTED					
k_p	θ_c	δ_{ec}	δ_{spc}	θ_c	δ_{ec}	δ_{spc}	N_{B1}	N_{B2}	N_{B3}
7	2.6	4.7	-0.8	1.7	7.0	-0.55	0.91	0.41	1.00
8	4.2	4.2	-2.0	2.0	7.4	-0.74	0.82	0.39	1.00
9	7.3	4.1	-2.9	4.8	8.8	-2.0	0.48	0.36	1.00
10	8.6	4.0	-3.8	5.2	9.0	-2.4	0.43	0.36	1.00
11	10.4	3.8	-5.6	5.3	9.6	-2.7	0.40	0.34	1.00
13	11.1	3.7	-6.4	5.8	9.8	-3.4	0.33	0.34	1.00
15	12.1	3.6	-8.1	6.2	10.0	-4.2	0.28	0.33	1.00

Table 4.3.3 shows the mean points of limit cycle oscillations for a range of pilot gains. The first three columns of data in both the SIMULATED and PREDICTED portion of the table are the mean points of oscillation for pitch attitude in degrees, elevator deflection in degrees, and stick position in inches. The last three columns show the amount of offset limiting present in each of the saturation elements.

It can be seen from Table 4.3.2 that for low pilot gains (k_p less than 9 lb/deg) limit cycle oscillations are dominated by elevator deflection and rate limiting. This is evident by examining the values of N_A. As pilot gain increases all saturation elements begin to experience fairly high amounts of saturation, but the elevator rate limiter is always the

most dominant. The nature of these aircraft oscillations can be seen in Figures 4.3.3 through 4.3.5.

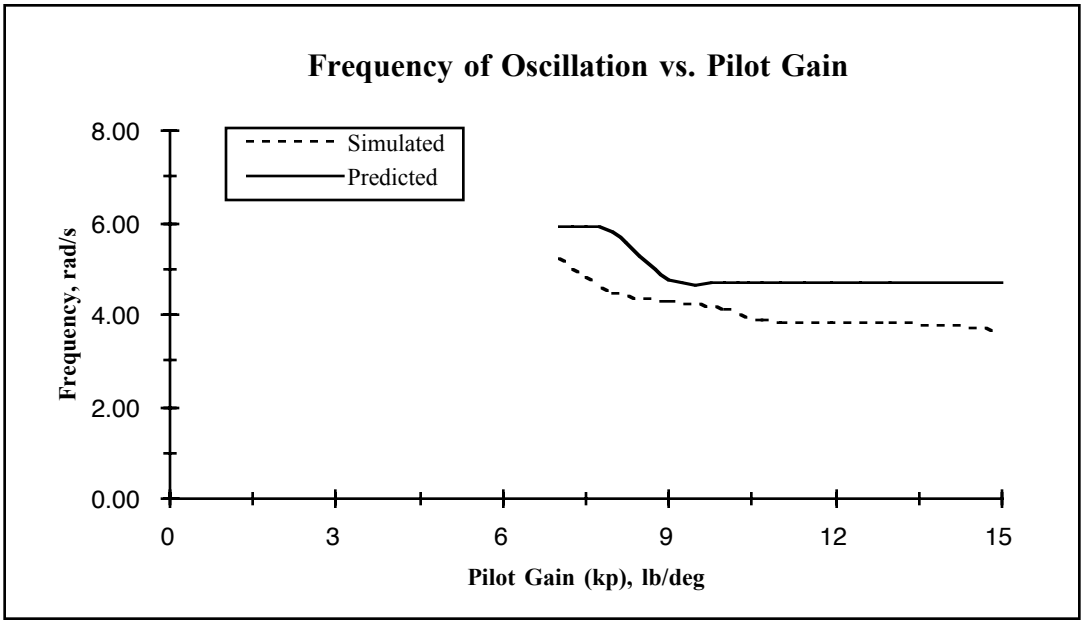

Figure 4.3.3 Frequency of Oscillation for NT-33A with Asymmetric Stick Position, Asymmetric Elevator Deflection, and Elevator Rate Limiting

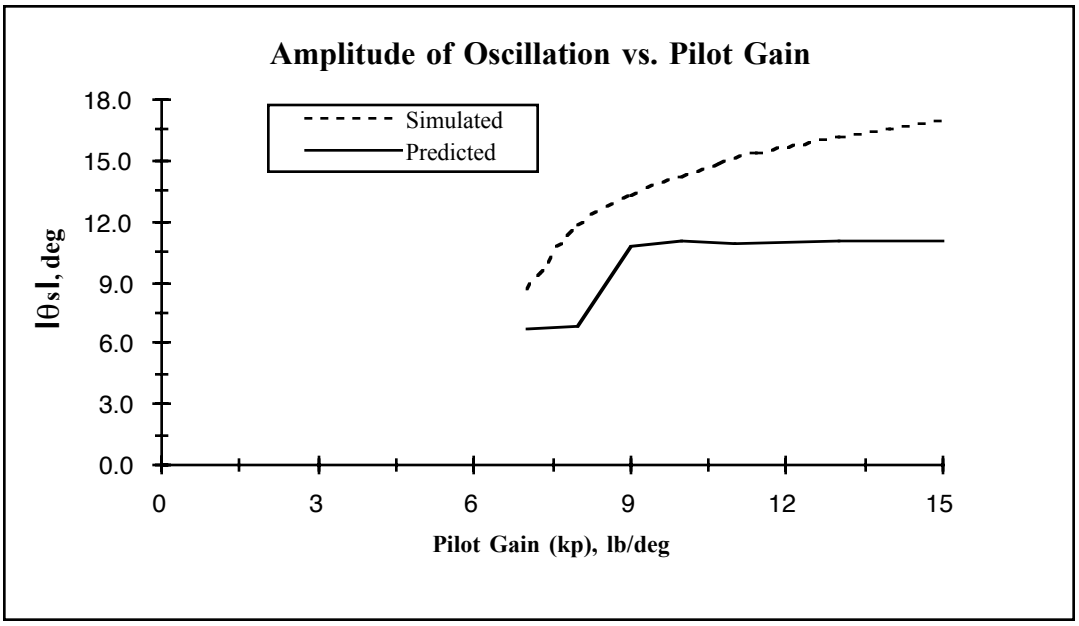

Figure 4.3.4 Amplitude of Pitch Attitude Oscillation for NT-33A with Asymmetric Stick Position, Asymmetric Elevator Deflection, and Elevator Rate Limiting

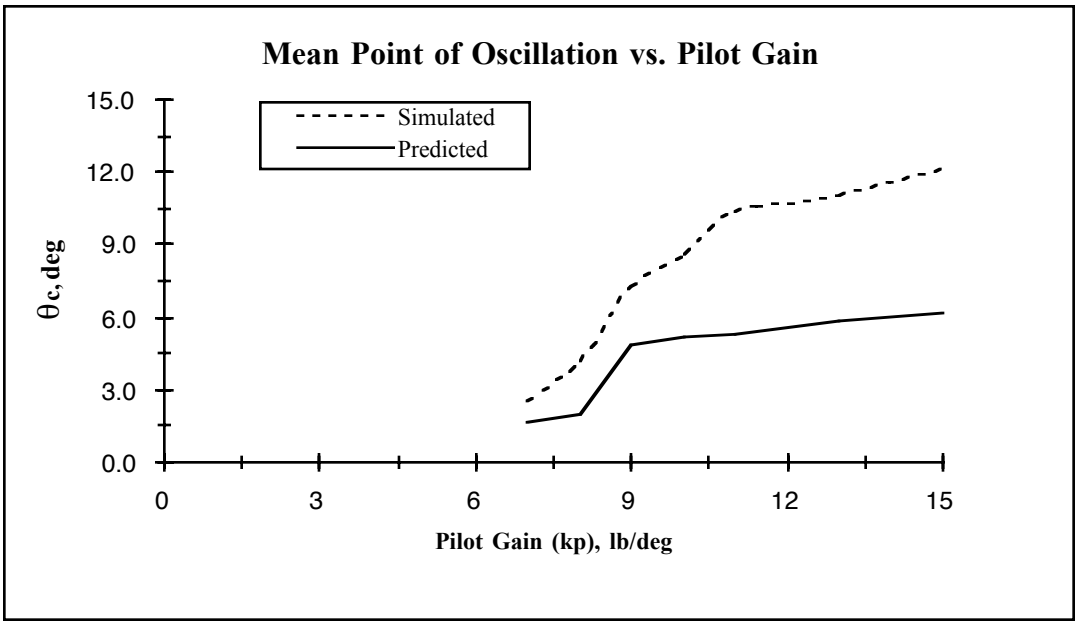

Figure 4.3.5 Mean Point of Pitch Attitude Oscillation for NT-33A with Asymmetric Stick Position, Asymmetric Elevator Deflection, and Elevator Rate Limiting

Frequencies of limit cycle oscillation for a range of pilot gains can be seen in Figure 4.3.3. Low pilot gains give an initial frequency of oscillation of about 6 rad/s. Note that as pilot gain is increased the frequency of oscillation decreases only slightly.

Aircraft pitch attitude oscillations are depicted by Figures 4.3.4 and 4.3.5. Figure 4.3.4 shows amplitude of pitch attitude oscillation for a range of gains, and Figure 4.3.5 shows mean point of pitch attitude oscillation for a range of gains. It can be seen from these figures that the mean point of oscillation is a large percentage of the amplitude of oscillation. Even at low pilot gains (k_p = 7 lb/deg) the mean point of oscillation is almost 25% of the amplitude. Mean point of oscillation exceeds 50% of the amplitude of oscillation rather quickly as pilot gain is increased. Also, note that changes in both amplitude and mean point of oscillation due to pilot gain changes are most dramatic in the region of small pilot gains (k_p = 7 - 9 lb/deg). The region of larger pilot gains is characterized by smaller changes in amplitude and mean point of oscillation due to changes in pilot gain.

Figures 4.3.6 and 4.3.7 depict the prelimited stick position oscillations.

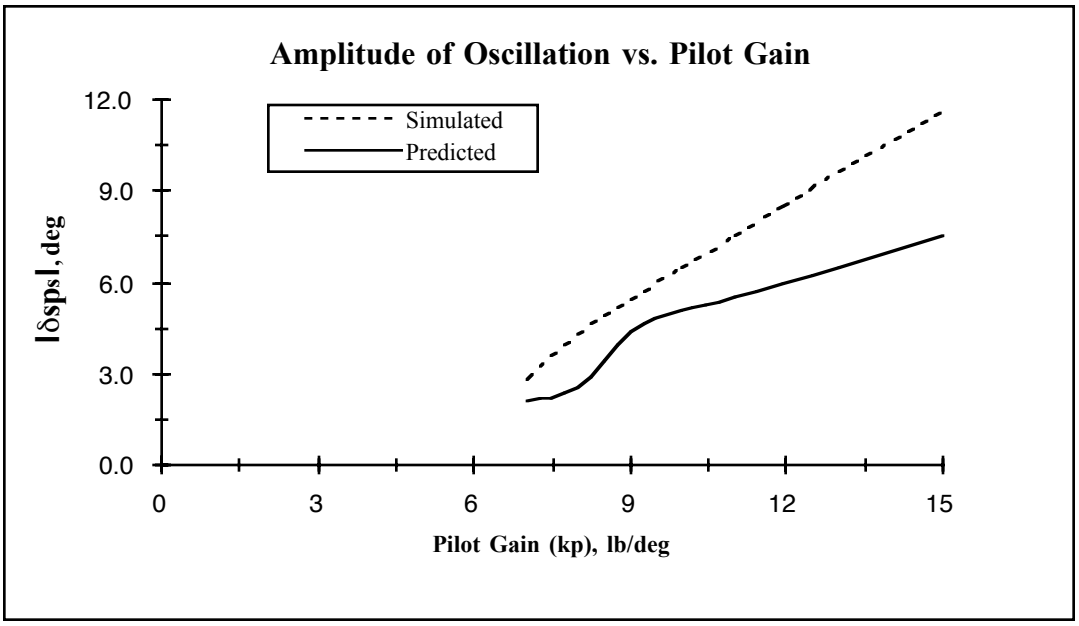

Figure 4.3.6 Amplitude of Stick Position Oscillation for NT-33A with Asymmetric Stick Position, Asymmetric Elevator Deflection, and Elevator Rate Limiting

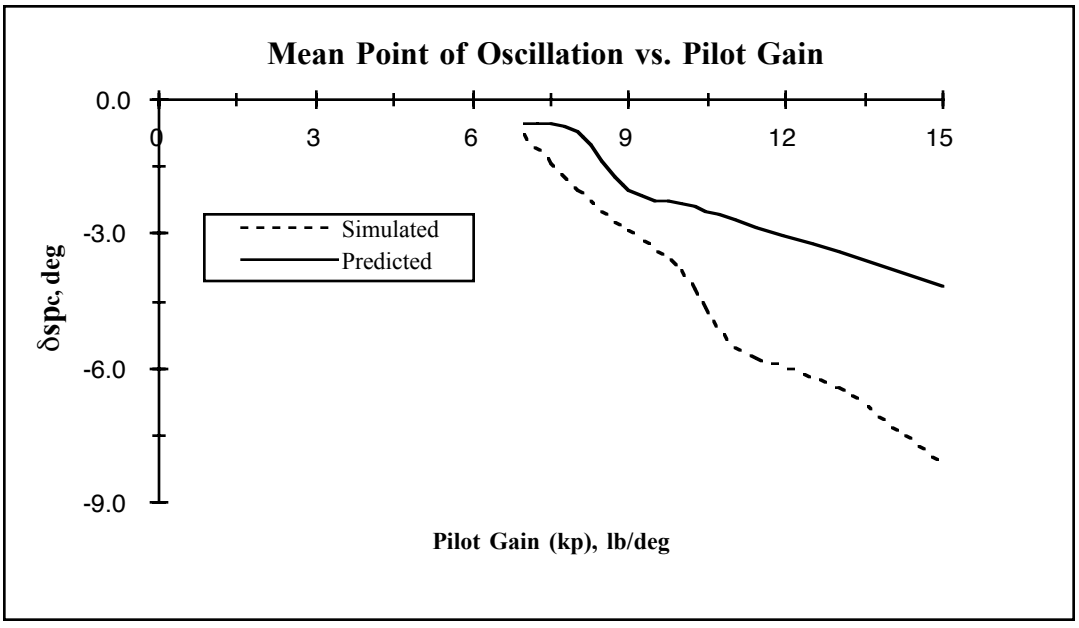

Figure 4.3.7 Mean Point of Stick Position Oscillation for NT-33A with Asymmetric Stick Position, Asymmetric Elevator Deflection, and Elevator Rate Limiting

Figure 4.3.6 shows amplitude of stick position oscillation for a range of pilot gains, and Figure 4.3.7 shows mean point of stick position oscillation for a range of pilot gains. Both amplitude and mean point of oscillation steadily become greater in magnitude for increasing pilot gain. Mean point of oscillation begins at about 20% of the amplitude and, as pilot gain is increased, quickly grows greater than 50% of the amplitude.

Figures 4.3.8 and 4.3.9 depict the prelimited elevator position oscillations.

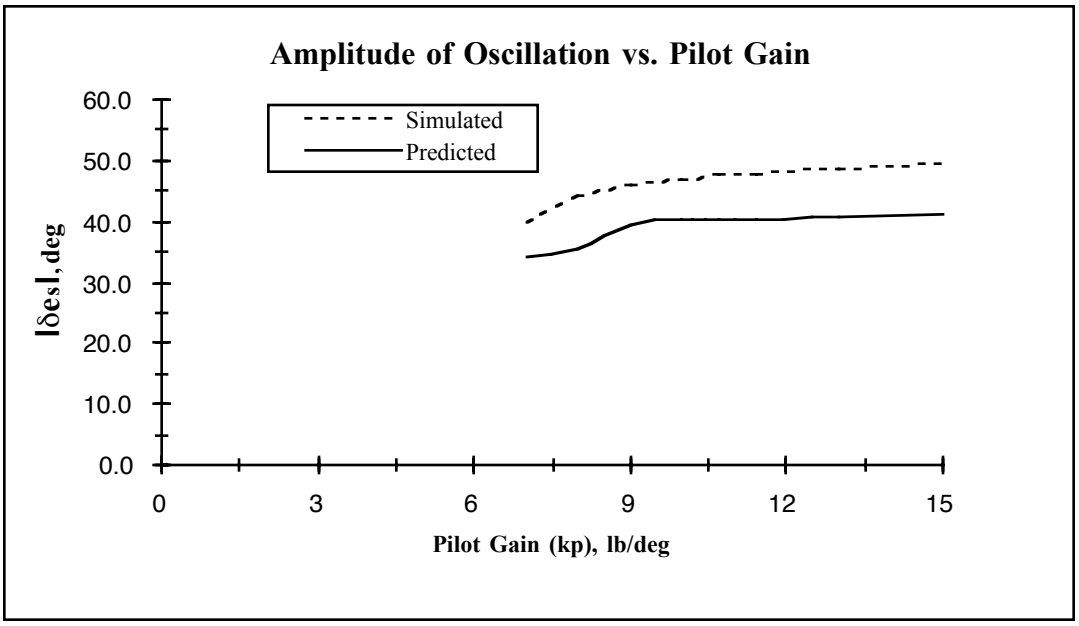

Figure 4.3.8 Amplitude of Elevator Deflection Oscillation for NT-33A with Asymmetric Stick Position, Asymmetric Elevator Deflection, and Elevator Rate Limiting

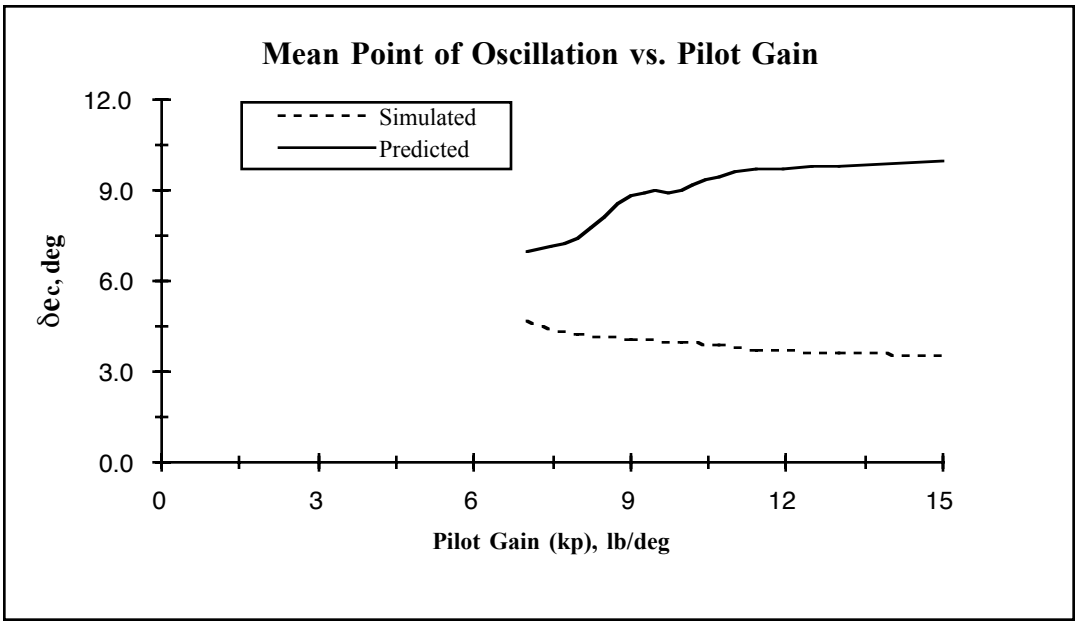

Figure 4.3.9 Mean Point of Elevator Deflection Oscillation for NT-33A with Asymmetric Stick Position, Asymmetric Elevator Deflection, and Elevator Rate Limiting

Figure 4.3.8 shows amplitude of stick position oscillation for a range of pilot gains, and Figure 4.3.9 shows mean point of stick position oscillation for a range of pilot gains. Both the simulated and predicted amplitude of stick position oscillation increase slowly for increasing pilot gain. However, predicted mean point of oscillation increases slowly for increasing pilot gain while simulated mean point of oscillation decreases slowly for increasing pilot gain. This discrepancy can be attributed to the highly nonlinear behavior of the stick position oscillations. This behavior is illustrated by Figure 4.3.10.

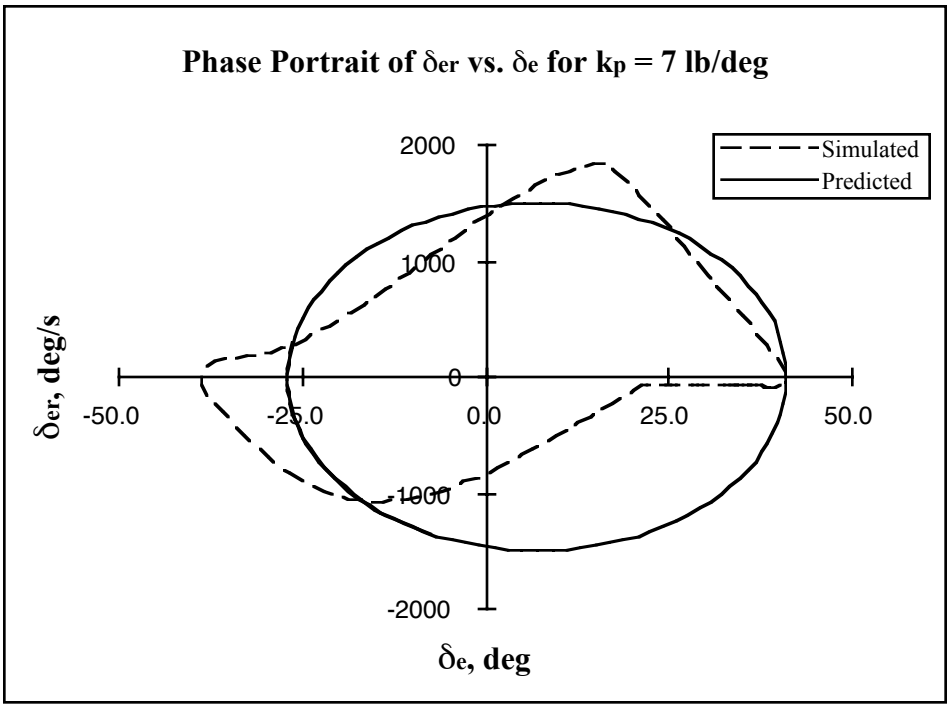

Figure 4.3.10 Phase Portrait of δ_{er} vs. δ_e for a pilot gain of k_p = 7 lb/deg

Figure 4.3.10 is a phase portrait of the elevator oscillations during a limit cycle created by a pilot gain of 7 lb/deg. Note that even at this low pilot gain the simulated oscillation is highly nonlinear. Once again, the DIDF prediction method attempts to represent this behavior as an ellipse.

Although not all components of the oscillation are accurately predicted, the overall prediction of limit cycle oscillations is reasonably good. The DIDF method gives the most accurate results for low pilot gain limit cycle oscillations. As pilot gain is increased, these approximations are not as accurate. Examples of this trend can be seen in the Appendix which depicts oscillation characteristics.

Another interesting outcome of the addition of the elevator rate limit is that of the appearance of a higher frequency limit cycle oscillation. This limit cycle is much less dominant and appears only for a pilot gain close to 9 lb/deg. Table 4.3.4 and 4.3.5 show simulated and predicted results for this limit cycle.

Table 4.3.4 Simulated and Predicted High Frequency Limit Cycle Solution for the NT-33A

	SIMULATED				PREDICTED						
k_p	ω	$\lvert\theta_s\rvert$	$\lvert\delta e_s\rvert$	$\lvert\delta sp_s\rvert$	ω	$\lvert\theta_s\rvert$	$\lvert\delta e_s\rvert$	$\lvert\delta sp_s\rvert$	N_{A1}	N_{A2}	N_{A3}
9	8.3	2.6	18.3	1.1	7.8	3.5	24.6	1.4	1.00	0.80	0.79

Table 4.3.5 Simulated and Predicted High Frequency Limit Cycle Solution for the NT-33A

	SIMULATED			PREDICTED					
k_p	θc	δe_c	δsp_c	θc	δe_c	δsp_c	N_{B1}	N_{B2}	N_{B3}
9	0.1	0.6	-0.02	0.4	2.7	-0.16	1.00	0.65	1.00

Table 4.3.4 shows frequency and amplitudes of oscillation for the high frequency limit cycle oscillation and Table 4.3.5 shows the associated mean points of oscillation. Note that during this oscillation the predicted stick position is not limited at all. The amount of saturation in the elevator deflection and rate limits is rather low, as well. These

facts indicate that the predicted oscillation will be fairly representative of the simulated limit cycle.